PHYSICAL REVIEW A **70**, 041401(R) (2004)

Ionization dynamics of extended multielectron systems

M. Kitzler,[1,*] J. Zanghellini,[1] Ch. Jungreuthmayer,[1] M. Smits,[2] A. Scrinzi,[3] and T. Brabec[1,†]
[1]*Center for Photonics Research, University of Ottawa, Ottawa, Ontario, Canada*
[2]*Department of Physics and Astronomy, Vrije Universiteit Amsterdam, Amsterdam, The Netherlands and Steacie Institute for Molecular Sciences, National Research Council Canada, Ottawa, Ontario, Canada*
[3]*Photonics Institute, Vienna University of Technology, Vienna, Austria*
(Received 28 June 2004; published 15 October 2004)

Ionization of multielectron systems is investigated by using one-dimensional, multiconfiguration time-dependent Hartree-Fock calculations. Our analysis reveals the key physical processes underlying ionization of complex systems. The laser-induced multielectron dynamics, and therewith the ionization process, depend on the ratio of laser frequency (ω_0) to plasmon frequency (ω_p). In the overresonant limit ($\omega_0 \gg \omega_p$), tunnel ionization is destroyed and ionization takes place by a classical over the barrier mechanism. In the underresonant regime ($\omega_0 \ll \omega_p$), tunnel ionization remains dominant, but is weakened by a polarization-induced growth of the tunneling barrier.

DOI: 10.1103/PhysRevA.70.041401 PACS number(s): 42.50.Hz, 33.80.Rv, 82.50.Hp

The numerical investigation of ionization dynamics in multielectron systems is at the forefront of quantum physics [1]. Due to the complexity of the problem the use of approximations is indispensable. The most commonly used simplification is the single active electron (SAE) approximation, which is based on the assumption that only the valence electron interacts with the laser electric field. SAE theories have proven very successful in explaining ionization in noble gas atoms [2,3] and in small molecules [4,5]. Recent experiments in large molecules [6–9] clearly reveal the breakdown of the SAE approximation. This has raised the challenge to understand the limits of the SAE approximation and to develop more elaborate multielectron theories.

Here a theoretical investigation of ionization of complex systems is presented, based on one-dimensional (1D) multiconfiguration time-dependent Hartree-Fock (MCTDHF) calculations [10]. MCTDHF is a further development of the time-dependent Hartree-Fock method [11] and is currently the only method that enables calculation of the nonperturbative dynamics of few-electron systems, taking full account of electron correlation. Our analysis reveals the key physical processes underlying ionization of complex systems.

The first major result of this Rapid Communication is a demonstration of the dependence of tunnel ionization on system size and spatial structure. The potential barrier becomes more transparent for increasing system size. As a result, a larger part of the bound state wave function leaks under the barrier into the classically forbidden region, resulting in an enhancement of tunnel ionization. Ionization in complex materials is usually analyzed by comparing experiments with atomic ionization (ADK) theory [6,7]. The observed dependence shows that ADK theory has to be corrected for the specific structure. Only then can multielectron effects be extracted from measurements.

The second major result is the dependence of ionization on the ratio of laser frequency (ω_0) to the resonance frequency (ω_p) of collective electron motion. This ratio determines the dynamic polarizability and therewith the response of the electrons to the laser field, which strongly influences ionization. We identify two distinct ionization mechanisms in the over ($\omega_0 \gg \omega_p$) and underresonant regime ($\omega_0 \ll \omega_p$).

The third major result is a new ionization mechanism in the overresonant limit. For $\omega_0 \gg \omega_p$ the electrons move 180° out of phase with the laser field, and away from the tunneling barrier. As a result, tunnel ionization is destroyed and a classical ionization mechanism, dubbed laser dephasing heating (LDH), becomes dominant. For infrared laser radiation, the overresonant limit occurs in semiconductor materials and in nanostructures. Our investigation extends the physics of quantum dots and quantum wells into the strong field regime, a so far largely unexplored research area. An understanding of strong field effects such as ionization is essential, as they set the ultimate limit to the largest field strengths applicable to nanostructures.

The fourth major result demonstrates a modified tunneling mechanism in the underresonant limit that explains the reduction of ionization observed in large molecules [7,8]. In the underresonant limit, the electrons are pushed towards the tunneling barrier, creating a polarization that increases the tunneling barrier and reduces ionization. We find an increase of the saturation intensity of ionization by a factor of 5. This is in good agreement with typical experimental results [6,7], supporting the validity of our 1D analysis.

Our analysis is based on the solution of the Schrödinger equation for the 1D, f-electron Hamiltonian with the potential (atomic units are used throughout, unless otherwise stated) $V=\Sigma_{i=1}^{f}[V_n(x_i)-x_iE(t)+\Sigma_{j>i}^{f}V_e(x_i-x_j)]$. Here, V_n refers to the nuclear binding potential, $V_e=1/\sqrt{(x_i-x_j)^2+a_e}$ represents the electron-electron interaction potential, a_e is a shielding parameter, and $E(t)$ is the laser field. The f-electron wave function is calculated by the MCTDHF ansatz [10],

$$\Psi(x_1,\ldots,x_f;t)=\sum_J A_J(t)\varphi_{j_1}(x_1;t)\ldots\varphi_{j_f}(x_f;t). \qquad (1)$$

Here, $J=j_1,\ldots,j_f$ is a multi-index with $j_i\in\{1,..,n\}$. The expansion coefficients A_J are fully antisymmetric with re-

*Email address: kitzler@tuwien.ac.at
†Email address: brabec@uottawa.ca

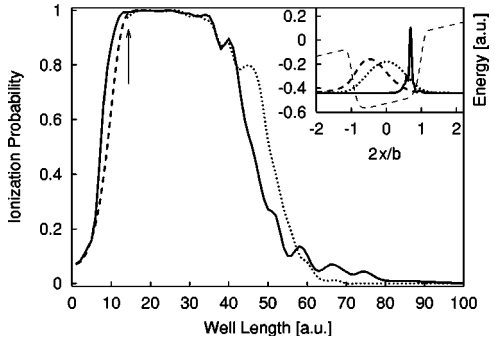

FIG. 1. Quantum mechanical (full line), analytical [Eq. (2), dashed line], and classical (dotted line) ionization probability versus potential length b of an electron in a square well potential with depth A. A is chosen for each b to keep $I_p=0.25$ constant. Inset: Field-free ground state (dotted line), electron probability distribution at the laser pulse peak for $b=10$ (thick dashed line) and for $b=55$ (full line). The narrow dashed line presents a schematic of the potential. Energy is plotted versus distance normalized to potential length.

spect to their indices, i.e., $A_{j_1,\ldots,j_i,\ldots,j_k,\ldots,j_f}=-A_{j_1,\ldots,j_k,\ldots,j_i,\ldots,j_f}$. Both, the coefficients $A_{j_1,\ldots,j_f}$ and the $n \geqslant f$ expansion functions φ_j are time dependent and are determined by the Dirac-Frenkel variational principle $\langle \delta\Psi | i\partial_t - H|\Psi\rangle = 0$. The spin is included in the calculations, although it has been dropped in our notation for the sake of simplicity. In the limit $n\to\infty$ the expansion Eq. (1) becomes exact. We perform calculations for $f=1$, $n=1$, and for $f=4$, $n=8$. In the multielectron case, a further increase of n changes the ionization yield by less than ±0.5% indicating convergence to the exact four-dimensional (4D) wave function. The Schrödinger equation is solved on a 1D grid with a uniform grid spacing of 0.15 and 4000 grid points. To avoid reflection at the simulation boundaries, complex absorption potentials are used. For details of the numerical technique see Ref. [10].

Both single- and multielectron phenomena play an important role in complex materials. As both effects are closely intertwined, it is helpful to investigate them separately. Therefore, the paper is organized in the following way. The first part is devoted to the investigation of single electron effects in complex systems. In the second part the analysis is generalized to the multielectron case.

In Fig. 1 the ionization yield of a single electron in a square-well potential is depicted as a function of the well width b. For different values of b, the well-depth A is adjusted to keep the ionization potential $I_p=0.25$ constant. The laser field has the form $E=E_0 f(t)\cos(\omega_0 t)$ with wavelength $\lambda_0=800$ nm, and peak intensity $I=5\times10^{13}$ W/cm^2. The full width at half maximum (FWHM) duration of the Gaussian envelope $f(t)$ is chosen $\tau=10$ fs.

The arrow in Fig. 1 denotes the well width at which the laser frequency is equal to the transition frequency between the ground and the first excited state, i.e., $\omega_0=\omega_{01}$. As ω_{01} decreases with increasing b, the areas left and right of the arrow present the underresonant ($\omega_0<\omega_{01}$) and the overresonant ($\omega_0>\omega_{01}$) limit of laser-matter interaction. In atomic ionization theory, the Keldysh parameter [2] $\gamma=\omega_0\kappa/E_0 \ll 1$ indicates that ionization occurs predominantly via tunneling, where $\kappa=\sqrt{2I_p}$. For our parameters $\gamma=0.34$, so that tunnel ionization is expected to occur over the whole range. As γ is independent of b, atomic ionization theory [3] would predict a constant ionization probability in Fig. 1.

Contrary to expectations, a strong increase of the ionization probability is observed in Fig. 1 in the underresonant limit, in agreement with experiments [12]. The process not properly accounted for by atomic tunneling theory [3] is identified by generalizing the theory to a square well potential, which yields

$$w(t) = c(b)\kappa^2 \exp\left(-\frac{2\kappa^3}{3E(t)}\right),$$

$$c(b) = \frac{\cos^2(kb/2)\exp(\kappa b)}{\cos^2(kb/2) - \kappa b/2 + (\kappa/2k)\sin(kb)}. \qquad (2)$$

Here, $k=\sqrt{2(A-I_p)}$, and the structural correction factor c is determined by the magnitude of the absolute squared of the asymptotic ground state wave function in the classically nonallowed region. In the limit of $b\to 0$, $A\to-\infty$, the parameter $c\to 1$, and the tunneling rate of a 1D delta-function potential is recovered. The major difference to atomic ionization theory is that c in Eq. (2) depends on the structure of the system. With increasing b a larger portion of the ground state wave function can slip into the classically nonallowed region increasing c. The exponential dependence of c explains the sharp rise for $b<6$. For larger well widths ($6\leqslant b\leqslant 12$) the numerical and analytical ionization yields differ by up to a factor of 2. The difference arises from the fact that the density of bound states increases with b and so does the electron mobility. This is not included in Eq. (2). With increasing mobility the electron is pushed more strongly towards the tunneling barrier. As a result, the wave function under the barrier increases (see the dashed line in the inset of Fig. 1), and ionization is enhanced.

A surprising feature in Fig. 1 is the drop of the ionization yield in the overresonant regime. Ionization is inhibited, because the electron moves against (180° out of phase with) the laser field away from the tunneling barrier (see the full line in the inset of Fig. 1). This response is known from overresonantly driven oscillators [13]. In the overresonant limit, the electron dynamics becomes close to that of a free electron which moves 180° out of phase with the laser field.

The wave function in the inset of Fig. 1 is plotted for $b=55$ (full line). As the wave function is pushed away from the tunneling barrier, one would expect ionization to be suppressed. Still, appreciable ionization takes place. Inspection of the wave-function dynamics shows that the electron absorbs energy, when it hits the potential well barrier. The electron collides during each half cycle with the potential barrier and absorbs energy, until its energy is large enough to escape over the barrier. The strength of LDH scales with the ratio of electron excursion amplitude to well width. Therefore, ionization in Fig. 1 drops to zero for increasing b.

LDH is a classical process. This follows from a comparison of the quantum result to classical simulations. A set of trajectories, with starting points covering the classically allowed part of the potential well, is launched. The trajectories

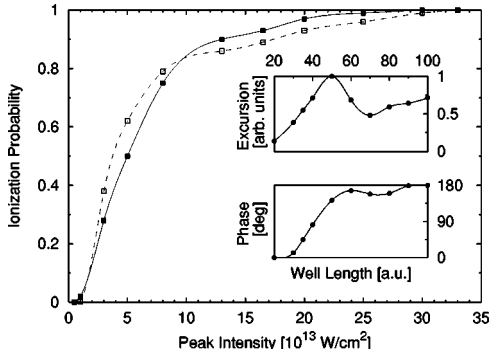

FIG. 2. Quantum mechanical (full squares) and classical (open squares) ionization probability versus laser intensity of a square well potential with four electrons. Inset: normalized excursion of the center of gravity of the electron density at the peak of the laser pulse (upper part), phase relation between laser electric field and the center of gravity motion of the electron density (lower part) versus b (intensity, $I=5\times10^{13}$ W/cm^2).

are weighted with the probability of the ground state wave function. The initial velocity is calculated by $v_i = \pm\sqrt{2(I_p-A)}$. The classical equations of motion are solved subject to these initial conditions. The ionization probability is determined by the sum over the weight of the trajectories that are free after the laser pulse. The result is depicted by the dotted line in Fig. 1. The agreement with the quantum results is good, proving the classical nature of LDH ionization.

A generalization of our analysis to four interacting electrons shows that ionization by LDH and suppression of tunnel ionization also exists in the multielectron case. This is corroborated by the excellent agreement between quantum and classical calculations for the four-electron system depicted in Fig. 2, where we show the ionization probability as a function of laser peak intensity. The parameters are $a_e=1$, $I_p=0.448$, $b=100$, $\lambda_0=800$ nm, Gaussian envelope, and FWHM $\tau=6$ fs.

In multielectron systems the transition between under- and overresonant behavior is more complex than in the single-electron case discussed above, as, in addition to single-electron excitations, plasmon effects play a strong role. A plasmon oscillation is a collective excitation in which the electrons respond to the laser field in a coherent fashion, like a single macroparticle. Analysis of the electron density in Fig. 2 reveals that the collective electron motion dominates over single-electron excitations. The inset depicts the normalized excursion amplitude of the center of gravity of the electron density at the peak of the laser pulse (upper part), and the phase relation between laser and electron oscillation (lower part) as a function of b for $I=5\times10^{13}$ W/cm^2.

The collective electron motion depends on the system length b, and therewith on the electron density. This is a typical signature of plasmon oscillations: the plasmon frequency (ω_p) grows with the square root of the electron density. With decreasing b the electron density and the plasmon frequency are increased, and the electron motion changes from overresonant, 180° out of phase to underresonant, in-phase motion with the laser electric field. At $b\approx45$ the excursion is maximum and the phase difference is ≈90°, indicating resonance between laser and plasmon oscillation, i.e., $\omega_p=\omega_0$. The change from overresonant to underresonant behavior can be understood in terms of the dynamic polarizability, $\alpha(\omega)=\alpha_0/(\omega_p^2-\omega^2)$, with α_0 the static polarizability. For $\omega_0\ll\omega_p$ the dynamic polarizability goes over into the static polarizability, whereas for $\omega_0\gg\omega_p$ the polarizability changes sign, explaining the 180° phase change.

Typical plasmon frequencies of large molecules, of clusters, and of condensed matter lie between ≈0.035 (1 eV) and ≈1 (27.2 eV). Therefore, with near-infrared lasers the overresonant limit is not reached in most of these media. Suppression of tunnel ionization and LDH are important in nanostructures, such as quantum wells and quantum dots, and in semiconductors [14], where electron density and plasmon frequency can be tailored by doping. The dependence of the electron dynamics and of ionization on laser wavelength and electron density opens ways to control carrier dynamics in nanostructures.

In the remainder of the paper we generalize ionization in the underresonant limit to multielectron systems. This limit applies to the interaction of infrared laser light with most molecules and clusters. Even in the underresonant regime, the plasmon frequency plays an important role in ionization. Recently it was suggested that nonadiabatic transitions to excited states can take place [7], resulting in an enhancement of ionization. Our analysis shows that the plasmon resonance plays a dominant role in the nonadiabatic regime of ionization. Here, we focus on the adiabatic limit $\omega_0\ll\omega_p$, where transitions to excited states, such as the plasmon resonance, can be neglected, and $\alpha(\omega)\approx\alpha_0$.

In order to describe the asymptotic potential of molecules correctly, the target is modeled by a chain of four Coulomb nuclei with one electron per nucleus, i.e., $V_n(x_i)=-\Sigma_{j=1}^{f}1/\sqrt{(x_i-jd)^2+a_n}$, with the distance $d=3.5$ between adjacent nuclei. The nuclear and electron shielding parameters are chosen to be $a_n=2.25$ and $a_e=0.81$. The ionization potential of the highest occupied molecular orbital (HOMO) is $I_p=0.261$. Finally, the laser pulse is Gaussian, $\lambda_0=1500$ nm, and $\tau=10$ fs.

The multielectron effects are identified by a comparison to SAE-electron calculations. The SAE potential is assumed to be a smoothed Coulomb potential outside the leftmost and rightmost nucleus of the molecule, and constant inside. The well depth is chosen to obtain the same I_p as for the four-electron molecule.

The comparison of SAE (empty squares) and four-electron (full triangles) calculations in Fig. 3 reveals that multielectron effects dominate tunnel ionization. Despite the same ionization potential, the four-electron saturation intensity of ionization is by a factor of 5 larger than the SAE result. Taking the 1D nature of our analysis and experimental uncertainties into account, this result is in reasonable agreement with measurements, where an increase of the saturation intensity by factors of 3–8, as compared to SAE theory, was obtained [6–8].

It is interesting to make the same comparison for He. From comparison with experiments it is known that the SAE

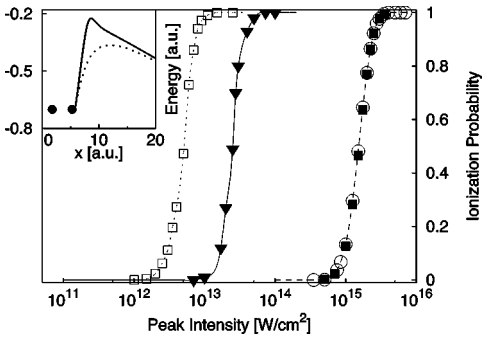

FIG. 3. Ionization probability of the HOMO electron versus laser peak intensity. Full triangles: four-electron molecule; empty squares: corresponding SAE calculation. Full squares: two-electron He; empty circles: He SAE calculation. Inset: tunneling barrier in the presence (full) and absence (dotted) of electron polarization.

approximation works well for noble gases. For $a_e=0.55$ and $a_n=0.55$ the ionization potential of He, $I_p=0.9$, is obtained. The two-electron (full squares) and the SAE (empty circles) calculation in Fig. 3 coincide, giving proof of the validity of the SAE approximation.

Finally, the physical origin of the violation of the SAE approximation in complex systems needs to be identified. In the single-electron case we have seen that the electron is pushed against the tunnel barrier by the laser field. In the multielectron case the same process polarizes the molecule. The resulting modification of the molecular potential results in an increase of the tunneling barrier, as is shown in the inset of Fig. 3. The inset shows the potential of nuclei, remaining bound electrons, and laser field as felt by the tunneling electron (full line). The dotted potential is calculated from the field-free four-electron wave function, where the molecule's polarization is zero. The full line denotes the potential obtained from the four-electron wave function at the peak of the laser pulse, where the polarization is maximum. Comparison of the two curves reveals a polarization caused increase of the molecular tunneling barrier.

Ionization in 1D complex multielectron systems was investigated by using the MCTDHF method. We identified the main physical effects determining ionization in multielectron systems, which are size and geometry, electron mobility, and polarizability. Our analysis revealed ionization mechanisms playing an important role in a broad range of research areas, from strong field molecular physics to nanotechnology. Despite the 1D nature of our calculations, reasonable agreement with experiments shows that the essential effects of tunnel ionization can be captured by a 1D analysis. The results of our analysis present a guideline for the generalization of existing ionization theories to more complex systems. Finally, they will be helpful for the design of future strong field experiments in a broad range of areas, including nanophysics and molecular physics.

Invaluable discussions with P. B. Corkum, A. Stolow, and D. M. Rayner are acknowledged. This work was supported by NSERC, PRO, and by the Austrian Research Fund, Projects F01115 and F01611.

[1] A. D. Bandrauk and H.-Z. Lu, *Special Volume of Handbook of Numerical Analysis*, edited by P. G. Ciarlet, (Elsevier Science, Amsterdam, 2003), Vol. X.
[2] L. V. Keldysh, Sov. Phys. JETP **20**, 1307 (1965).
[3] M. V. Ammosov, N. B. Delone, and V. P. Krainov, Sov. Phys. JETP **64**, 1191 (1986).
[4] C. Guo, Phys. Rev. Lett. **85**, 2276 (2000).
[5] X. M. Tong, Z. X. Zhao, and C. D. Lin, Phys. Rev. A **66**, 033402 (2002).
[6] S. M. Hankin *et al.*, Phys. Rev. Lett. **84**, 5082 (2000).
[7] M. Lezius *et al.*, J. Chem. Phys. **117**, 1575 (2002).
[8] V. R. Bhardwaj, P. B. Corkum, and D. M. Rayner, Phys. Rev. Lett. **91**, 203004 (2003).
[9] A. N. Markevitch *et al.*, Phys. Rev. A **68** 011402(R) (2003).
[10] J. Zanghellini *et al.*, J. Phys. B **37**, 763 (2004).
[11] K. C. Kulander, Phys. Rev. A **36**, 2726 (1987).
[12] M. J. DeWitt and R. J. Levis, Phys. Rev. Lett. **81**, 5101 (1998).
[13] L. D. Landau and E. M. Lifshitz, *Mechanics* (Pergamon Press, New York, 1976).
[14] L. Jacak, P. Hawrylak, and A. Wojs, *Quantum Dots* (Springer-Verlag, Berlin, 1998).